

Spiral morphology and galactic shear rate

Robert J.J. Grand ^{*}, Daisuke Kawata, Mark Cropper

Mullard Space Science Laboratory, University College London, Holmbury St. Mary, Dorking, Surrey, RH5 6NT

20 September 2012

ABSTRACT

Spiral galaxies are observed to exhibit a range of morphologies, in particular in the shape of spiral arms. A key diagnostic parameter is the pitch angle, which describes how tightly wound the spiral arms are. Observationally and analytically, a correlation between pitch angle and galactic shear rate has been detected. For the first time, we perform a suite of N-body simulations to calculate and compare the pitch angles of both individual density waves and overall spiral structure by use of two independent techniques. We find that higher galactic shear rates produce more tightly wound spiral arms, both in individual mode patterns (density waves) and in the overall density enhancement. Although the mode pattern pitch angles by construction remain constant with time, the overall logarithmic spiral arm winds over time, which is consistent with both the observational scatter in pitch angle versus shear seen from observations, and the recent idea that multiple mode patterns may interfere with each other to create apparently winding spiral arm structures.

Key words: galaxies: evolution - galaxies: kinematics and dynamics - galaxies: spiral - galaxies: structure

1 INTRODUCTION

Spiral arms are the defining structure of any spiral galaxy. Simulations have shown that their transient nature (e.g. Sellwood 2010, 2011) invokes significant effects on the dynamics of baryonic matter in the galaxy, particularly in the disc plane (e.g. Goldreich & Lynden-Bell 1965; Sellwood & Binney 2002; Roškar et al. 2008; Grand et al. 2012a,b), namely the well known radial migration phenomenon, as well as heating and possibly disc thickening (e.g. Schönrich & Binney 2009; Loebman et al. 2011; Solway et al. 2012; Minchev et al. 2012). Because all of this is directly dependent on the spiral structure, it can be expected that different spiral morphologies imprint the dynamical history of a galaxy in different ways and degrees.

There are several reported causes of spiral structure, such as external perturbations from tidal interactions with a satellite galaxy (e.g. Holmberg 1941; Toomre & Toomre 1972; D’Onghia et al. 2010; Dobbs et al. 2010; Purcell et al. 2011). The presence of a central bar may also be a driver of density waves and lead to grand design spiral galaxies (Buta et al. 2005; Salo et al. 2010; Athanassoula 2012, and references therein). Spiral structure may also grow from internal disc instabilities such as local Toomre instabilities, or arise from the presence of a large mass perturber such as giant molecular

clouds (D’Onghia et al. 2012). Reported physical mechanism(s) responsible for driving the spiral structure include swing amplified (Julian & Toomre 1966; Toomre 1981) density waves (Lin & Shu 1964; Goldreich & Lynden-Bell 1965; Lynden-Bell & Kalnajs 1972; Sellwood & Binney 2002), multiple spiral/bar wave modes (Sparke & Sellwood 1987; Masset & Tagger 1997; Minchev & Quillen 2006; Minchev & Famaey 2010; Quillen et al. 2011; Roškar et al. 2011) and co-rotating structures (Wada et al. 2011; Grand et al. 2012a,b; Fujii & Baba 2012). Recent observations have highlighted the possible existence of both density wave and co-rotating type spiral arms in nature (e.g. Merrifield et al. 2005, 2006; Meidt et al. 2008, 2009; Egusa et al. 2009; Foyle et al. 2011; Speights & Westpfahl 2011; Ferreras et al. 2012), some of whom find evidence against the classic spiral density wave theory either by use of the offset method (Egusa et al. 2009) that measures the offset of star forming tracers (e.g. Foyle et al. 2011; Ferreras et al. 2012) or the some form of the Tremaine-Weinberg Equations (e.g. Merrifield et al. 2005, 2006; Speights & Westpfahl 2011), and some who find evidence for multiple density waves (Meidt et al. 2008, 2009). Whether the mechanism for driving spirals be some form of density waves or otherwise, it appears there is some mechanism that shapes galaxy morphology into a preferentially tight or open structure.

A correlation between the shape of the galactic rotation curve and the orientation (pitch angle) of a spiral arm-like density enhancement was derived analytically by

^{*} rjg2@mssl.ucl.ac.uk

Julian & Toomre (1966) (see also Fuchs et al. 2005), who used the Hill approximations applied to the shearing sheet, in which the evolution of the response density to a large perturbing mass is calculated as swing amplification amplifies the density around the perturber. They showed that the density enhancement in this context is predicted to show smaller pitch angles (i.e. more tightly wound structure) with increasing amount of shear present.

This correlation is supported observationally as well. Seigar et al. (2005) looked at a sample of several barred galaxies and used a Fourier analysis to draw the spiral shape, and found evidence for the shear rate dependency of the spiral arm pitch angle. This survey was later extended and the conclusion strengthened by Seigar et al. (2006).

In this paper, we aim to test both theoretical and observational predictions by running a suite of N-body simulations, each with varying shear rates. For the first time we investigate the pitch angles of individual spiral patterns in N-body simulations by isolating the patterns from the system and calculating the spiral phase of the m -th mode. Because we assume a density wave nature in order to study individual patterns, the pitch angle is assumed to be constant. We find that the discs of higher shear rate exhibit systematically smaller pitch angles as predicted from the analytical studies mentioned above. We also trace the overall spiral feature and its pitch angle as a function of time. When measured in this way, we find that the pitch angle decreases with time because the apparent spiral arm features behave as short-lived transient spirals (Sellwood 2010, 2011), that appear to wind in simulations (Grand et al. 2012a,b). The observational work of Seigar et al. (2006), which measures the pitch angle and shear rate of many spiral galaxies, reveals several different observed pitch angles for a given shear rate. We find that this scatter in pitch angle versus shear appears to be consistent with the range of pitch angles that the winding arms in our simulations exhibit. The pitch angle evolution might also shed light on whether or not the spiral arm can be an apparently winding structure owing to the interference of multiple wave mode patterns (Comparetta & Quillen 2012).

The simulations are described in Sec. 2, the analysis and results are described in Sec. 3 followed by the discussion in Sec. 4.

2 SIMULATIONS

The simulations in this paper are performed with a hierarchical Tree N-body code (Kawata & Gibson 2003). We perform three simulations, each of which consists of a spherical static dark matter halo (and a spherical static stellar bulge component in two of the simulations) and a live stellar disc.

The dark matter halo density profile follows that of Navarro et al. (1997):

$$\rho_{\text{dm}} = \frac{3H_0^2}{8\pi G} \frac{\Omega_0 - \Omega_b}{\Omega_0} \frac{\rho_c}{cx(1+cx)^2}, \quad (1)$$

where ρ_c is the characteristic density described by Navarro et al. (1997), the concentration parameter, $c = r_{200}/r_s$, and $x = r/r_{200}$. The scale length is r_s , and r_{200} is the radius inside which the mean density of the dark mat-

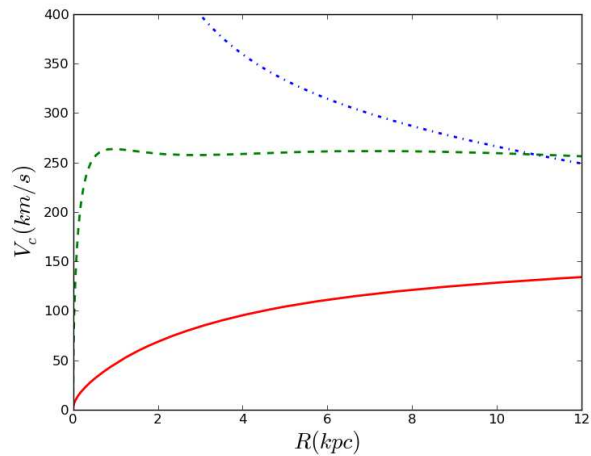


Figure 1. The circular velocity at $t = 0$ for simulation R (solid), F (dashed) and K (dot-dashed) lines respectively.

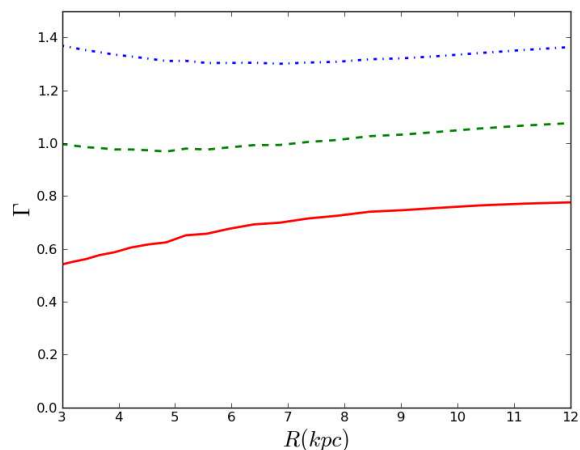


Figure 2. Galactic shear rate for simulation R (solid red), F (dashed green) and K (dot-dashed blue) lines respectively.

ter sphere is equal to $200\rho_{\text{crit}}$ (where $\rho_{\text{crit}} = 3H_0^2/8\pi G$; the critical density for closure):

$$r_{200} = 1.63 \times 10^{-2} \left(\frac{M_{200}}{h^{-1}M_\odot} \right)^{\frac{1}{3}} h^{-1} \text{kpc}. \quad (2)$$

We assume $\Omega_0 = 0.266$, $\Omega_b = 0.0044$ and $H_0 = 71 \text{ km s}^{-1} \text{ Mpc}^{-1}$.

The spherical static stellar bulge component is modelled by the Hernquist profile (Hernquist 1990), which is described by:

$$\rho_b(r) = \frac{M_b}{2\pi} \frac{a}{r} \frac{1}{(r+a)^3}, \quad (3)$$

where M_b is the total bulge mass and a is the scale length. The scale length is set to the effective radius, $R_e = 1.8153a$. We apply a compacting factor, b , to scale from the empirical relation of the bulge effective radius (Shen et al. 2003):

Simulation	$M_d(M_\odot)$	$R_d(\text{kpc})$	$M_{vir}(M_\odot)$	c	$M_b(M_\odot)$	b
R	1.0×10^{10}	3.5	2.5×10^{12}	5	-	-
F	5.0×10^{10}	3.5	1.5×10^{12}	15	4.0×10^{10}	0.5
K	5.0×10^{10}	3.5	1.0×10^{11}	15	1.0×10^{11}	0.01

Table 1. Table of initial model parameters for simulation R, simulation F and simulation K.

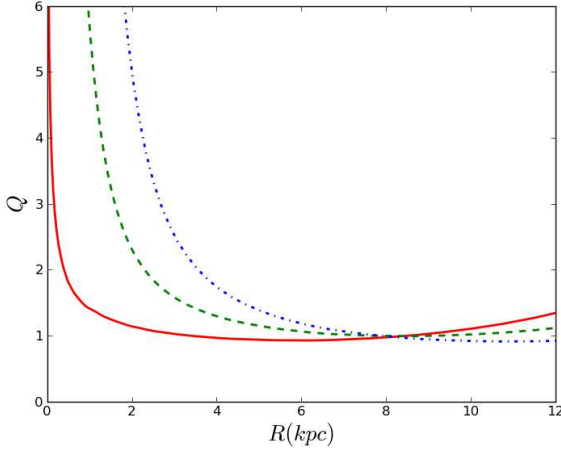


Figure 3. Toomre stability parameter, Q , at $t = 0$ for simulation R (solid red), F (dashed green) and K (dot-dashed blue) lines respectively.

$$R_{e,0} = 4.16 \left(\frac{M_b}{10^{11} M_\odot} \right). \quad (4)$$

Hence, the resultant scale-length is defined by $a = bR_{e,0}/1.8153$.

The stellar disc is assumed to follow an exponential surface density profile:

$$\rho_{d,*} = \frac{M_{d,*}}{4\pi z_{d,*} R_{d,*}} \text{sech}^2 \left(\frac{z}{z_{d,*}} \right) \exp \left(-\frac{R}{R_{d,*}} \right). \quad (5)$$

We use $N = 1 \times 10^6$ particles for each simulation to describe the disc. We apply a fixed softening length for star particles with the spline softening suggested by Price & Monaghan (2007). The softening length for galaxies F and K is 340 pc, and for simulation R it is 200 pc. The model parameters for the simulations are summarised in Table 1, and the rotation curves are shown in Fig. 1. The rotation curve that rises with increasing radius (simulation R) is produced by setting a large halo mass with a low concentration parameter, c , in order to extend mass to the outer regions of the disc. Because of such a low concentration of dark matter mass in the central region, the disc mass must be lowered in order to prevent a bar from forming (Ostriker & Peebles 1973). In this way, we avoid the added complication of the bar component and restrict the study to spiral galaxies only. To produce the flat (simulation F) and keplerian-like (simulation K) rotation curves, a bulge component is included. For simulation K, this is a very compact and massive bulge. Although this case is unrealistic, we include it in order to emphasise the effect of galactic shear on spiral morphology.

The radial profile of the galactic shear rate at $t = 0$, given by $\Gamma = 1 - (R/V_c)(dV_c/dR)$, for each simulation is shown in Fig. 2.

Julian & Toomre (1966) note that the response density can be weakly dependent on the Q stability parameter (defined as $Q = \sigma_{R\kappa}/3.36G\Sigma$). Therefore, we set the initial Q value for all our simulations (Fig. 3) to approximately 1 over the radial range $4 < R < 12$ kpc, so as to minimise any effect of this global parameter.

3 RESULTS AND DISCUSSION

Here we present the analysis and results of our two techniques for measuring pitch angles: mode pattern analysis and apparent spiral arm peak trace method. An important difference between these techniques worth noting is that the mode pattern analysis focuses only on individual density waves that may be present in the stellar disc, whereas the apparent spiral arm peak trace method analyses the spiral density enhancement as a whole.

Before we describe these two analysis techniques, we outline the method of pitch angle calculation. First, assume the positional information of a density enhancement is known. Then, the pitch angle can be expressed in terms of the position in polar coordinates:

$$\phi = \arctan \frac{\Delta R}{\Delta d_\theta}, \quad (6)$$

where the distance, d_θ , is the spatial distance in the azimuthal direction defined as $d_\theta = R\Delta\theta$. We assume logarithmic spiral arms, which means that we can use equation (6) to fit a linear function described by $R = bR\theta + a$, where b is the gradient of this line, equal to the tangent of the pitch angle. The next step is to recover the positional information of individual mode patterns and the apparent spiral arm peak in order to apply the linear fitting.

3.1 Pitch angles of mode patterns

In this section, we focus on the theory of swing amplified modes and their pitch angles. In the context of spiral density waves, swing amplification is the mechanism for the growth of density centred around a single co-rotation point. Studies of the shearing sheet approximation tell us that the orientation of the response density should depend on the rate of shear in the sheet. To extend this to galaxies, it is the morphology of the density wave that depends on the degree of galactic shear as a function of radius. The shape of a wave mode pattern is time independent, because each pattern has a constant pattern speed, therefore the pitch angle remains constant over time.

In this analysis, we focus on strong patterns because

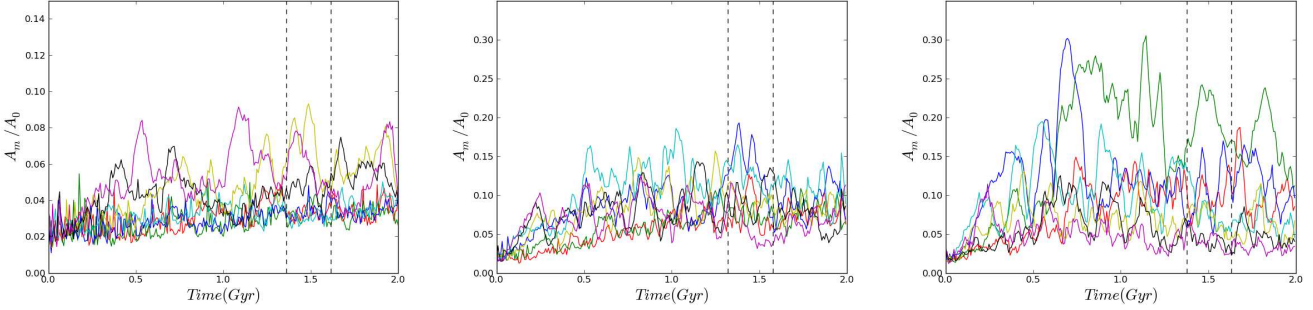


Figure 4. The amplitudes of spiral modes $m = 1$ (red), 2 (green), 3 (blue), 4 (cyan), 5 (yellow), 6 (black) and 7 (magenta), normalised to the axisymmetric $m = 0$ mode, as a function of time for simulation R (left), F (middle) and K (right) simulations. Vertical dashed lines represent the time window of the Fourier transform applied in Section 3.1. Strong contrasts are observed owing to the low $Q \sim 1$ parameter that induces spiral structure.

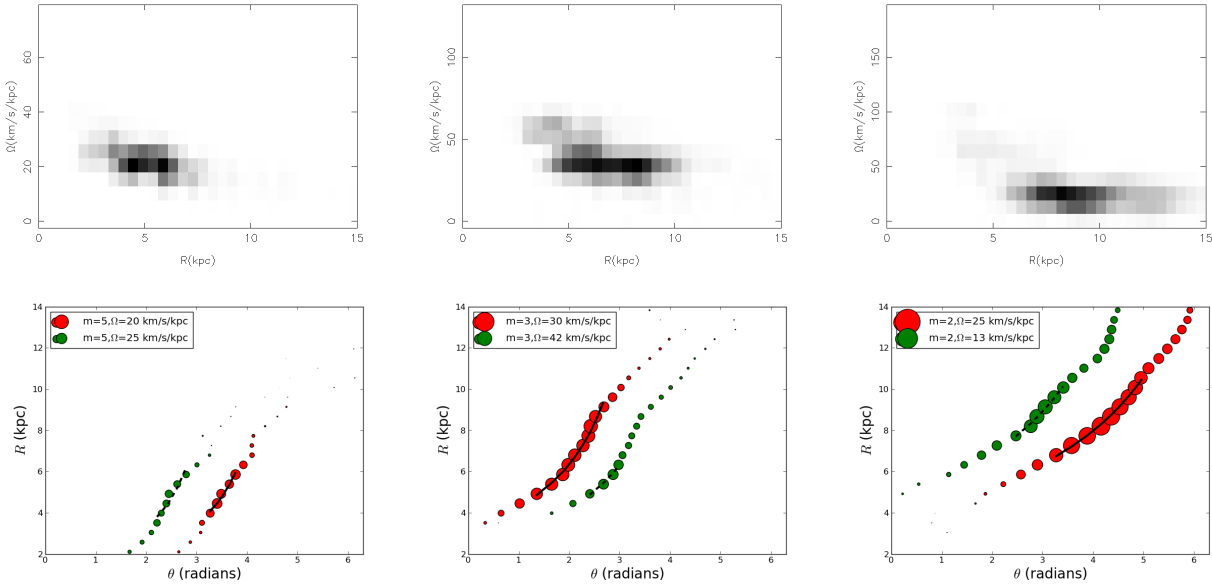


Figure 5. *Top panels:* Power spectra of simulation R for the $m = 5$ mode (left), F for the $m = 3$ mode (middle) and K for the $m = 2$ mode (right). Prominent ridges (dark pixels) span between 5 - 10 kpc in most cases. *Bottom panels:* Dominant mode pattern phase positions in the azimuth-radius plane for the corresponding spectra above. Each colour represents a different pattern. The symbol size reflects the relative amplitude of the pattern at a given position. The black lines show the lines of best fit for each pattern.

they give the greatest signal, whereas weaker patterns may be confused with noise. In order to find patterns of significant amplitude, we first search for dominant modes i.e. wave modes of m spiral arms that exhibit large amplitudes. The amplitude of a given wave mode, m , is calculated from the quantities:

$$W_c^m(r, t) = \sum_i^N \cos(m\theta_i),$$

$$W_s^m(r, t) = \sum_i^N \sin(m\theta_i), \quad (7)$$

where θ_i is the azimuthal angle between the radial vector of

the particle and a common reference vector. The amplitude is then calculated as:

$$A^m(r, t) = (W_c^m(r, t)^2 + W_s^m(r, t)^2)^{1/2}. \quad (8)$$

The maximum amplitude in a radial range 4–10 kpc is found for modes $m = 1 - 7$ over the entire 2 Gyr of the evolution for each simulation, shown in Fig. 4. It is evident that there are several modes present in each simulation. We focus our analysis on the most prominent modes in each simulation, i.e. $m = 5, 3$ and 2 for simulations R, F and K respectively.

The first step to recovering the positional information of a pattern of given multiplicity, m , from the simulation, is to compute the power spectra of the strong modes. We

compute the power spectra by taking the Fourier transform of each component in equation (7):

$$\begin{aligned}\tilde{W}_c^m(r, \omega) &= \int_{T_1}^{T_2} W_c^m(r, t) e^{i\omega t} h(t) dt, \\ \tilde{W}_s^m(r, \omega) &= \int_{T_1}^{T_2} i W_s^m(r, t) e^{i\omega t} h(t) dt,\end{aligned}\quad (9)$$

where $h(t)$ denotes the Hanning function. T_1 and T_2 denote the beginning and end of the time window of the Fourier transform, which is chosen to be at around a relatively late epoch of the simulation when the system is more stable than in earlier times (see dashed vertical lines in Fig. 4). It is also centred around a peak of the most dominant mode present in each case, and spans $\Delta t = 256$ Myr.

The amplitude in each frequency as a function of radius is then calculated via:

$$A^m(r, \omega) = (\tilde{W}_c^m(r, \omega)^2 + \tilde{W}_s^m(r, \omega)^2)^{1/2}. \quad (10)$$

For each of our galaxies, the power spectrum of the dominant mode is calculated from the square of the amplitude given in equation (10), and shown as a function of radius and the pattern speed, $\Omega = \omega/m$, in the top row of Fig. 5. Because simulations generally possess several patterns for a given mode that can overlap in radius (e.g. see Fig. 4 of Roškar et al. 2011), care must be taken when computing the spiral phase of a pattern. One should select individual patterns by isolating a horizontal ridge (a single pattern speed) over a radial range where the signal significantly stands out from the noise, and proceed to calculate the spiral phase of that pattern. In each of the galaxies, we lift the most dominant patterns (the darkest horizontal ridges in the power spectra in the top panel of Fig. 5) and look at the three quantities, $\tilde{W}_c^m(r, \omega)$, $\tilde{W}_s^m(r, \omega)$ and $A^m(r, \omega)$ on the real and imaginary axis for each radial pixel in a ridge. We are able to calculate the spiral phase as:

$$\theta_{sp}^m(r, \omega) = \arctan\left(\frac{\tilde{W}_s^m(r, \omega)}{\tilde{W}_c^m(r, \omega)}\right), \quad (11)$$

from which we can convert to real phase position within the domain 0 to 2π , by dividing by the multiplicity, m : $\theta_p(r, \Omega) = \theta_{sp}^m(r, \omega)/m$. Therefore, by considering only the Fourier coefficients of a single given ω whose amplitudes stand out from the noise in the power spectrum, we may retrieve $\theta_{sp}^m(r, \omega)$ using equation (11), and calculate the corresponding phase position of a single pattern as a function of radius and then the pitch angle. The phase positions for each case are shown in the bottom row of Fig. 5. The size of each point represents the amplitude, $A^m(r, \omega)$, normalised to the largest amplitude of all the patterns shown in a given mode. Therefore the size of each point reflects the relative strength of a pattern at a given radius. The linear fitting of a constant pitch angle of equation (6) described at the beginning of the section is applied to points which exceed 70% of the maximum amplitude for each pattern. We applied a variety of these cuts and found that this cut best fit all the data. The best fit lines shown in Fig. 5 fit the points very well, and produce reliable pitch angles, whose averages are 12.9° , 20.3° and 33.1° for shear rates of ~ 1.3

(simulation K), ~ 1.0 (simulation F) and ~ 0.7 (simulation R) respectively. This reproduces the expected trend of pitch angle vs. shear very well: the density wave mode patterns display more tightly wound structure when the shear rate is higher.

3.2 Pitch angle of apparent spiral structures

It is now interesting to look at the pitch angle of the apparent spiral arms in our simulations for two reasons: the apparent density enhancement of the spiral arms may manifest from more than one overlapping and interfering wave pattern (Grand et al. 2012a; Comparella & Quillen 2012) like the ones seen in the upper panels of Fig. 5. The other reason is that if the apparent spiral arms wind with time (previously reported in Grand et al. 2012a,b; Wada et al. 2011), the pitch angle must vary with time. This may have interesting consequences for observations of galaxy pitch angle vs. shear (Siegar et al. 2005, 2006), as winding spiral arms will show a range of pitch angles for a given shear rate, which will be reflected in observations of a galaxy sample.

The method we use to trace the spiral arm peak position is a density weighting method, in which we select a point near the spiral arm of interest at some start radius (~ 5 kpc), define an azimuth range that encapsulates the width of the spiral arm and weight by density to find the peak position (see Grand et al. 2012b, for more details). This is iterated over a radial range until the spiral arm peak position is drawn out. This is done over a range of snapshots between 1 and 2 Gyr of the simulation evolution and the pitch angles are calculated in the same way as the mode pattern pitch angles in Section 3.1.

Because the pitch angles of spiral arms appear to decrease as their evolution proceeds from birth to death i.e. the arm winds, care must be taken that spiral arms are not chosen at some special moment when they are at a particular stage of winding. To ensure that we measure pitch angles in an unbiased way, only those spiral arms that show a single density peak in the azimuthal direction for each radius in the specified radial range for fitting are chosen for measurement. This is a limitation of this method. Fig. 6 demonstrates an example of the application of the arm tracing criteria to one of the spiral arms in simulation K. Because it is possible to reliably trace spiral arms which show only single peak structure for the radial range considered for fitting, we reject those snapshots that show the spiral arm with messy or double peak structure, which typically occurs during spiral arm formation ($t = 1.152$ Gyr in Fig. 6) and after the arm shows bifurcation or breaking ($t = 1.2$ Gyr in Fig. 6).

The results for several spiral arms in each simulation are shown in Fig. 7. It is obvious that every spiral arm pitch angle decreases with time. This is consistent with winding, co-rotating spiral arms which have been reported in Wada et al. (2011) and Grand et al. (2012a,b). The mode pattern pitch angles calculated in the previous section are highlighted by the shaded regions in Fig. 7. The apparent pitch angle of any given spiral arm straddles the mode pattern pitch angle region calculated from the corresponding simulation. The overlap occurs close to the middle of the traceable time sequence of a spiral arm. A snapshot of a time when both pitch angles overlap for each simulation is shown in Fig. 8. The agreement between the mode pattern pitch angles and the

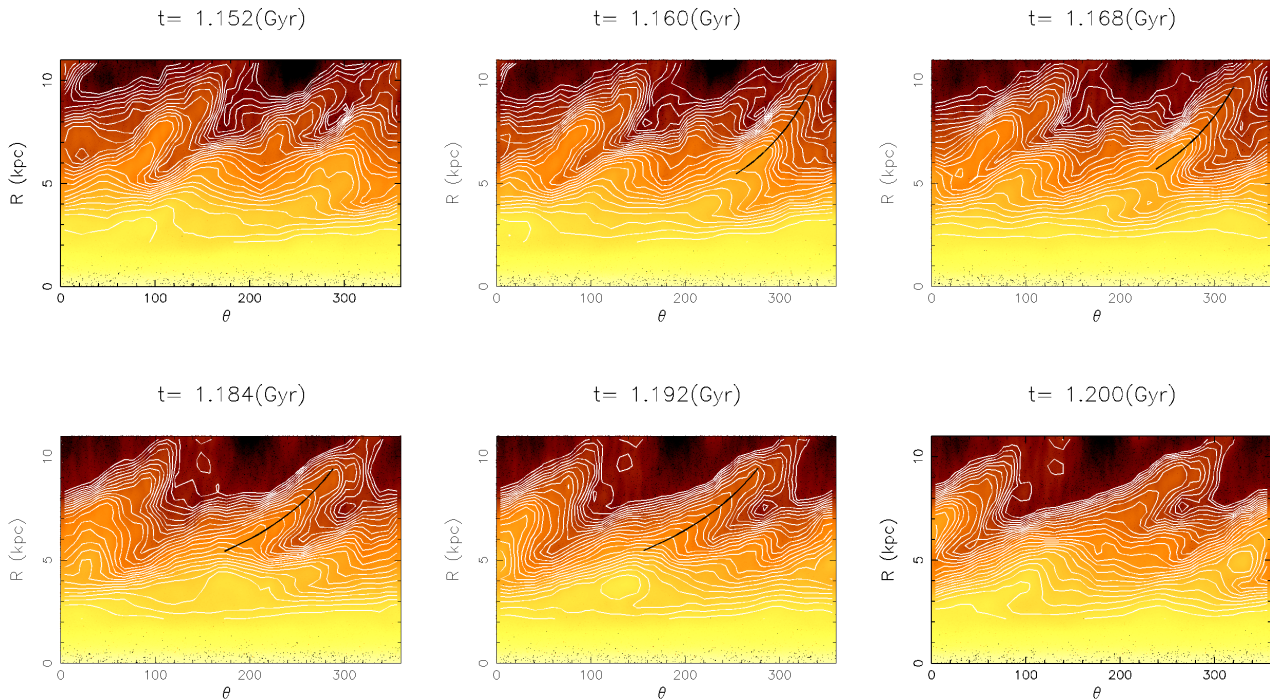


Figure 6. Snapshots of the disc density in polar coordinates. Density contours are overlaid in white. The traced spiral arm position is highlighted with a black line. Note the double peak structure at $R \sim 5.5$ and ~ 9 kpc at snapshots $t = 1.152$ and $t = 1.2$ Gyr, that prevents an unambiguous fitting to a single peak. This criteria defines the time range in which we can trace the spiral arm.

apparent spiral arm pitch angles, together with the presence of several patterns of seemingly varying pattern speeds is consistent with the idea that two or more density waves may periodically constructively interfere with one another to create a spiral arm. The apparent pitch angle begins larger than the mode pitch angle, and approaches the mode pitch angle while the density grows (constructive interfering). The waves then pass and move away from one another, which leads to a stretch in the azimuthal direction of the apparent spiral arm density. This produces a winding in the overall apparent spiral arm pitch angle. The co-rotating spiral arm features seen in previous simulations may be understood as the interference of multiple wave modes as noted by Grand et al. (2012a) who commented: “If there are indeed several wave modes present, it is evident that they must conspire in a specific way in order to produce a spiral arm feature that is apparently co-rotating”. It may be that the conspiracy is an interference mechanism of several wave mode patterns, each co-rotating at their respective radii of peak amplitude, that yields a near co-rotating pattern speed at the overlap regions (Comparetta & Quillen 2012). The growth of such wave mode patterns is naturally expected from swing amplification. However, the evolution of such modes should be non-linear and complicated (D’Onghia et al. 2012), which deserves further study. In this case, the wave mode patterns at the outer radii have lower pattern speeds than those at the inner radii i.e. $\Delta\Omega/\Delta R < 0$, so the evolution of the pitch angle may be represented by the time dependent gradient of the linear best fit line,

$$b(t) = \frac{\Delta R}{R(\Delta\theta_0 - \Delta\Omega t)}, \quad (12)$$

where $\Delta\Omega$ is the difference in pattern speed between different radii. Therefore, if $\Delta\Omega/\Delta R < 0$, b decreases with time, and hence the pitch angle decreases with time as well.

The pitch angles calculated from the overall density enhancement in Fig. 7, are plotted against galactic shear in Fig. 9. The range of the apparent pitch angle for a fixed shear rate appears to be similar to the scatter seen in the observed pitch angle-shear rate relation (e.g. Fig. 3 of Seigar et al. 2006). This indicates that spiral arms are in fact really winding, possibly as a consequence of multiple mode patterns interfering, and that observers are seeing spiral arms at snapshots at varying stages of their evolution, and therefore detect a range of pitch angles at a given rate of shear.

4 CONCLUSIONS

We have presented three N-body simulations each with different shaped rotation curves, and analysed the pitch angle of spiral arms and underlying mode patterns with two different techniques. We presented and compared the results of both techniques, and come to the following conclusions.

- (i) We calculate pitch angles of individual mode patterns for the first time by lifting their phase information directly out of the power spectrum of a strong mode multiplicity, and assuming logarithmic spiral arms in order to use the

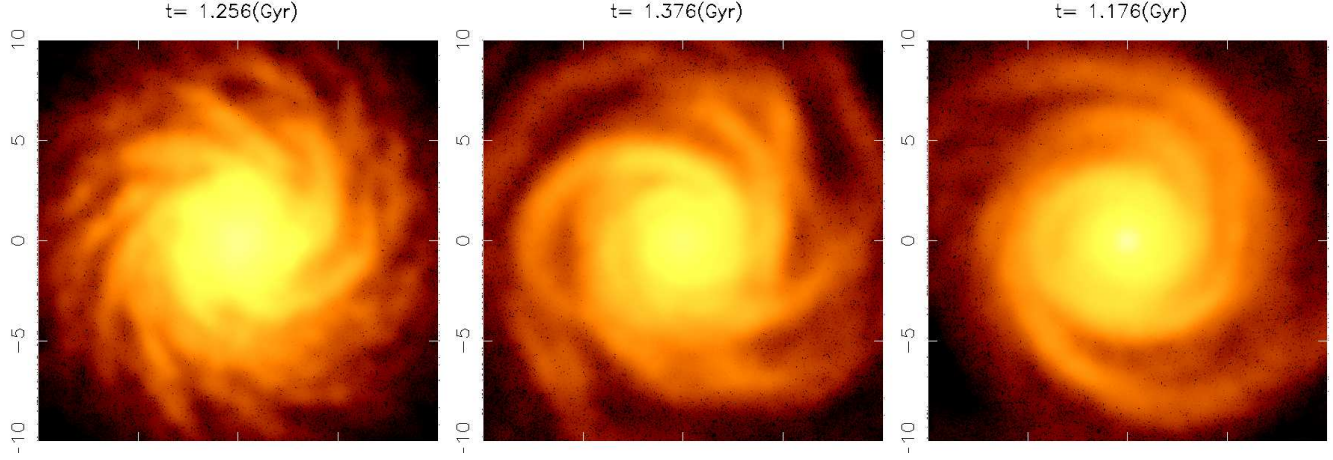


Figure 8. Face on view of each simulation (from left to right: simulations R, F and K) when the apparent spiral arm pitch angle coincides with the calculated mode pattern pitch angle. The degrees of spiral morphology are strikingly different: spirals become increasingly tight going from left to right.

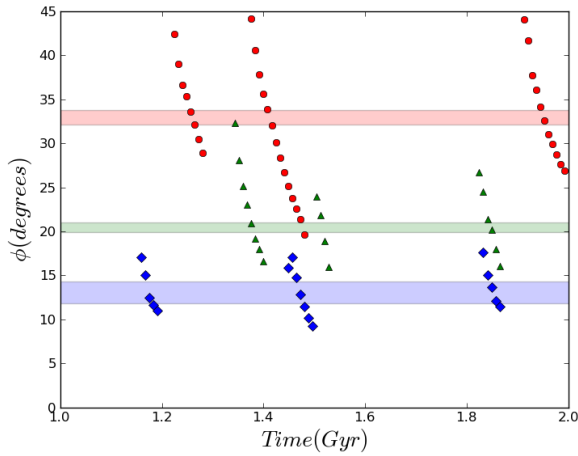


Figure 7. Pitch angle evolution of the apparent spiral arm for simulation R (circles), F (triangles) and K (diamonds). In all cases the pitch angle decreases with time, which indicates the winding nature of the overall density peak. The shaded horizontal regions represent the mode pattern pitch angles, determined from the patterns in Fig. 5 for simulations R (red), F (green) and K (blue). Note that the range of apparent spiral arm pitch angles clearly map out separate domains and straddle the mode pattern pitch angles of their respective galaxies.

linear fit to get a constant pitch angle from the gradient. We find the mode pitch angle is correlated with the rate of galactic shear: the pitch angle is smaller for higher galactic shear rate and vice versa. This is consistent with the analytical predictions based on swing amplification theory in Julian & Toomre (1966) and Fuchs et al. (2005).

(ii) Pitch angles of the spiral arm density enhancement itself are calculated in the same way from the density weighted position of the spiral arm peak. These pitch angles decrease with time, as the spiral arms grow from a relatively open morphology, then wind over time to become more tightly

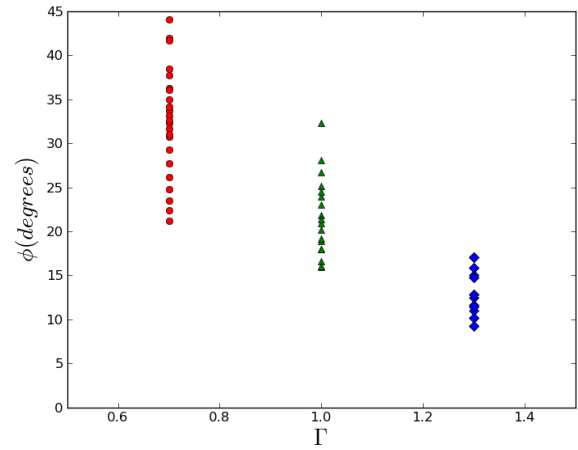


Figure 9. All calculated apparent spiral arm pitch angles plotted as a function of galactic shear for simulations R (red), F (green) and K (blue).

wound until they disrupt. This is consistent with previous simulations that reported winding and co-rotating spiral arms (Wada et al. 2011; Grand et al. 2012a,b).

(iii) The range of the variation of the pitch angles owing to the winding spiral arm features are similar to the scatter seen from the observed relation between the pitch angle and the shear rate in spiral galaxies. This indicates that real galaxies exhibit transient, winding spiral arms that may be caused by interfering spiral waves.

The pitch angle is a key structural parameter of spiral arms, which is shown to depend on the shape of rotation curve. In the context of both density wave mode patterns and the overall stellar density enhancement, the morphology of spiral arms is important to the evolution of disc stars that themselves give rise to the structure. Phenomena such as radial migration is likely to be dependent on the orientation

of the spiral arm against the orbit of stars, and hence the spiral morphology of the galaxy in general. The pitch angle of the spiral arm may therefore affect how much a star can migrate. It is possible that there are other criteria which a star must satisfy that, coupled with the spiral morphology, will determine the ability of a star to migrate radially. These criteria will be explored in a forthcoming paper.

ACKNOWLEDGEMENTS

First and foremost, the authors thank Jerry Sellwood for many useful suggestions and conceptually helpful discussions, particularly on the methodology. The authors acknowledge the support of the UK's Science & Technology Facilities Council (STFC Grant ST/H00260X/1). The calculations for this paper were performed on Cray XT4 at Centre for Computational Astrophysics, CfCA, of National Astronomical Observatory of Japan and the DiRAC Facility jointly funded by STFC and the Large Facilities Capital Fund of BIS. The authors acknowledge support of the STFC funded Miracle Consortium (part of the DiRAC facility) in providing access to the UCL Legion High Performance Computing Facility. The authors additionally acknowledge the support of UCL's Research Computing team with the use of the Legion facility. This work was carried out, in part, through the Gaia Research for European Astronomy Training (GREAT-ITN) network. The research leading to these results has received funding from the European Union Seventh Framework Programme ([FP7/2007-2013] under grant agreement number 264895.

REFERENCES

- Athanassoula E., 2012, MNRAS, p. L505
 Buta R., Vasylyev S., Salo H., Laurikainen E., 2005, AJ, 130, 506
 Comparetta J., Quillen A. C., 2012, ArXiv e-prints
 Dobbs C. L., Theis C., Pringle J. E., Bate M. R., 2010, MNRAS, 403, 625
 D'Onghia E., Vogelsberger M., Faucher-Giguere C.-A., Hernquist L., 2010, ApJ, 725, 353
 D'Onghia E., Vogelsberger M., Hernquist L., 2012, ArXiv e-prints
 Egusa F., Kohno K., Sofue Y., Nakanishi H., Komugi S., 2009, ApJ, 697, 1870
 Ferreras I., Cropper M., Kawata D., Page M., Hoversten E. A., 2012, MNRAS, 424, 1636
 Foye K., Rix H.-W., Dobbs C. L., Leroy A. K., Walter F., 2011, ApJ, 735, 101
 Fuchs B., Dettbarn C., Tsuchiya T., 2005, A&A, 444, 1
 Fujii M. S., Baba J., 2012, ArXiv e-prints
 Goldreich P., Lynden-Bell D., 1965, MNRAS, 130, 125
 Grand R. J. J., Kawata D., Cropper M., 2012a, MNRAS, 421, 1529
 Grand R. J. J., Kawata D., Cropper M., 2012b, ArXiv e-prints
 Hernquist L., 1990, ApJ, 356, 359
 Holmberg E., 1941, ApJ, 94, 385
 Julian W. H., Toomre A., 1966, ApJ, 146, 810
 Kawata D., Gibson B. K., 2003, MNRAS, 340, 908
 Lin C. C., Shu F. H., 1964, ApJ, 140, 646
 Loebman S. R., Roškar R., Debattista V. P., Ivezić Ž., Quinn T. R., Wadsley J., 2011, ApJ, 737, 8
 Lynden-Bell D., Kalnajs A. J., 1972, MNRAS, 157, 1
 Masset F., Tagger M., 1997, A&A, 322, 442
 Meidt S. E., Rand R. J., Merrifield M. R., 2009, ApJ, 702, 277
 Meidt S. E., Rand R. J., Merrifield M. R., Shetty R., Vogel S. N., 2008, ApJ, 688, 224
 Merrifield M. R., Rand R. J., Meidt S. E., 2005, in American Astronomical Society Meeting Abstracts Vol. 37 of Bulletin of the American Astronomical Society, Measuring Pattern Evolution: Winding Spiral Structure and Counter-Rotating Double Bars. p. 1313
 Merrifield M. R., Rand R. J., Meidt S. E., 2006, MNRAS, 366, L17
 Minchev I., Famaey B., 2010, ApJ, 722, 112
 Minchev I., Famaey B., Quillen A. C., Dehnen W., Martig M., Siebert A., 2012, ArXiv e-prints
 Minchev I., Quillen A. C., 2006, MNRAS, 368, 623
 Navarro J. F., Frenk C. S., White S. D. M., 1997, ApJ, 490, 493
 Ostriker J. P., Peebles P. J. E., 1973, ApJ, 186, 467
 Price D. J., Monaghan J. J., 2007, MNRAS, 374, 1347
 Purcell C. W., Bullock J. S., Tollerud E. J., Rocha M., Chakrabarti S., 2011, Nature, 477, 301
 Quillen A. C., Dougherty J., Bagley M. B., Minchev I., Comparetta J., 2011, MNRAS, 417, 762
 Roškar R., Debattista V. P., Quinn T. R., Stinson G. S., Wadsley J., 2008, ApJ, 684, L79
 Roškar R., Debattista V. P., Quinn T. R., Wadsley J., 2011, ArXiv e-prints
 Salo H., Laurikainen E., Buta R., Knapen J. H., 2010, ApJ, 715, L56
 Schönrich R., Binney J., 2009, MNRAS, 396, 203
 Seigar M. S., Block D. L., Puerari I., Chorney N. E., James P. A., 2005, MNRAS, 359, 1065
 Seigar M. S., Bullock J. S., Barth A. J., Ho L. C., 2006, ApJ, 645, 1012
 Sellwood J. A., 2010, ArXiv e-prints
 Sellwood J. A., 2011, MNRAS, 410, 1637
 Sellwood J. A., Binney J. J., 2002, MNRAS, 336, 785
 Shen S., Mo H. J., White S. D. M., Blanton M. R., Kauffmann G., Voges W., Brinkmann J., Csabai I., 2003, MNRAS, 343, 978
 Solway M., Sellwood J. A., Schönrich R., 2012, MNRAS, 422, 1363
 Sparke L. S., Sellwood J. A., 1987, MNRAS, 225, 653
 Speights J. C., Westpfahl D. J., 2011, ApJ, 736, 70
 Toomre A., 1981, in S. M. Fall & D. Lynden-Bell ed., Structure and Evolution of Normal Galaxies What amplifies the spirals. pp 111–136
 Toomre A., Toomre J., 1972, ApJ, 178, 623
 Wada K., Baba J., Saitoh T. R., 2011, ApJ, 735, 1